

<https://doi.org/10.1038/s42003-025-07939-7>

# The lifelong nonlinear development of spatial variability of brain signals

Chengxiao Yang<sup>1</sup>, Gen Li<sup>1</sup>, Xiujuan Jing<sup>1</sup>, Yifeng Wang<sup>1</sup> , Jin H. Yan<sup>2</sup> & Georg Northoff<sup>3</sup>

The physiological information carried by brain signals is distinguished by their mean and variability. Research has indicated that both the variability of local signals and the spatial mean of the whole-brain signal (known as the global signal, GS) are sensitive to brain development. This raises the question of whether the spatial variability of the whole-brain signal, referred to as global variability (GV), could potentially serve as a more specific marker of brain development. We first established the reliability of GV and its topography (GVtopo) using data from the Human Connectome Project (HCP). Then, we examined the age-related patterns of GV and GVtopo in the Nathan Kline Institute Rockland Sample (NKI-RS;  $N = 968$ , ages ranging from 6 to 85 years) and validated these findings in an independent dataset from Southwest University (SALD;  $N = 492$ , ages ranging from 19 to 80 years). Our results demonstrated the robustness of GV and GVtopo, with intra-class correlation coefficients surpassing 0.61. Both GV and GVtopo exhibited distinct non-linear developmental trajectories, differing from those of GS and its topography. Furthermore, GV demonstrated substantial age-predictive capability, underscoring its potential as a valuable marker of brain development and its significance for future age-related research.

The human brain evolves at multiple spatial and temporal scales, ranging from cells to the whole brain and milliseconds to the lifespan<sup>1,2</sup>. Resting-state functional magnetic resonance imaging (rs-fMRI) has emerged as a predominant approach for unveiling the age-related development of the human brain, from clusters of neurons to large-scale brain networks<sup>3–5</sup>. Using rs-fMRI, numerous studies have reported age-related changes in functional organization in almost all brain regions and networks<sup>3,6</sup>, emphasizing the necessity of whole-brain assessments in understanding brain development.

The global signal (GS) is formed by averaging the signals of all voxels in the brain. Initially, the GS is often treated as noise during image preprocessing<sup>7</sup>. However, recent studies indicate that GS regression should be applied cautiously as a data-cleaning strategy. This is because the GS, as a comprehensive measure of whole-brain signals, reflects neural activity along with non-neural signals, such as cardiac and respiratory noise<sup>8</sup>. Research involving mice<sup>9,10</sup>, monkeys<sup>11–13</sup>, and humans<sup>14–17</sup> has indicated that the GS, together with its topography (GStopo), represents an intrinsic spatiotemporal organization of the brain's architecture<sup>14,18,19</sup>. The GS and GStopo are genetically constrained and sensitive to the level/state of consciousness<sup>20,21</sup>, mental disorders<sup>22</sup>, and brain aging<sup>23–25</sup>. Just like the global average temperature, they hold a

unique value for our understanding of overall dynamics in brain function.

Despite GS providing spatially averaged amplitudes of brain signals, our knowledge of spatial variability remains limited. Recent rs-fMRI investigations have underscored that the mean and variability of time series of brain signals reflect distinct mechanisms associated with aging and cognition<sup>26–28</sup>. This distinction could also be applicable to spatial sequences. Exploring spatial variability may reveal neural mechanisms underlying cognition and mental disorders that mean values fail to capture<sup>29–31</sup>. For instance, evidence indicates that patients with generalized anxiety disorder show increased spatial variability<sup>29</sup>, demonstrating an inverted U-shaped relationship with anxiety levels. Spatial variability is generally lower in task states than resting states and is associated with more functional interactions between different brain regions<sup>30</sup>. Furthermore, rs-fMRI metrics have shown effective prediction of an individual's age, with temporal variability demonstrating significantly higher predictive accuracy than temporal mean for age estimation. Therefore, it is crucial to investigate whether spatial variability outperforms spatial mean in age prediction and whether they reflect different developmental characteristics of the brain.

To address these issues, we introduced the concepts of global variability (GV) and GV topography (GVtopo) and investigated their age effects

<sup>1</sup>Institute of Brain and Psychological Sciences, Sichuan Normal University, Chengdu, 610066, China. <sup>2</sup>Sports Psychology Department, China Institute of Sport Science, Beijing, 100061, China. <sup>3</sup>Mind, Brain Imaging and Neuroethics Research Unit, Institute of Mental Health Research, The Royal Ottawa Mental Health Centre and University of Ottawa, Ottawa, ON, K1Z 7K4, Canada. ✉e-mail: [wuyf@sicnu.edu.cn](mailto:wuyf@sicnu.edu.cn)

throughout the lifespan. Drawing on the algorithms of GS and GStopo<sup>32,33</sup>, we defined the standard deviation of whole-brain signals at each time point as GV and the Pearson correlation between GV and the spatial standard deviation of each brain region as GVtopo. Our initial focus was to evaluate the robustness of GV and GVtopo with the HCP dataset. Subsequently, we investigated the age effects of GV and GVtopo using a large sample dataset spanning the lifespan. To ascertain whether GV is an independent measure from GS, we conducted identical analytical procedures to assess the age correlation of GV after global signal regression (GSR) and to examine the developmental trajectory of GS after global variability regression (GVR). Our findings revealed distinct development patterns for GV and GS. Significantly, the regression of GS did not impact the development pattern of GV, and vice versa. This discovery strengthens the notion that GV contains age-related information independently of GS. Finally, we utilized GV and GVtopo as features in a support vector regression (SVR) analysis, revealing their ability to predict age effectively. Overall, our results suggest that GV and GVtopo represent unique developmental patterns of brain functional organization, providing valuable insights into the neural basis of age-related changes in brain function.

## Results

### The GV and GVtopo exhibited high degrees of test-retest reliability

We employed four runs of rs-fMRI data from the HCP dataset to examine the test-retest reliability of the GV and GVtopo. Both GV (ICC = 0.616) and GVtopo (ICC = 0.978) yielded good reliability (Fig. 1), surpassing the mean reliabilities of traditional functional connectivity<sup>34</sup> and brain activation<sup>35</sup>. As shown in Fig. 1B, the spatial distribution of GVtopo followed a ventromedial-dorsolateral pattern, with the lowest value located in the parahippocampal gyrus and the highest in the parietal cortex, distinct from the sensorimotor-association cortex pattern of GStopo<sup>36</sup>.

### The quadratic relationship between age and GV/GVtopo

As shown in Fig. 2, there was a significant positive quadratic effect between age and GV, characterized by its peak during early life and a subsequent decline with age, stabilizing at approximately 50. In contrast, the GS was essentially stable at all ages, consistent with the findings of Ao et al.<sup>25</sup>.

A curve-fitting analysis was conducted on both GVtopo and GStopo. As illustrated in Fig. 3B, the developmental trend of GVtopo displayed a U-shaped curve in the inferior frontal gyrus, thalamus, insula, amygdala, parahippocampus, and hippocampus, while an inverted U-shaped curve was observed in the posterior superior temporal sulcus, inferior parietal lobule, precuneus, and cingulate gyrus. After GSR, the age-related fit demonstrated a similar pattern of curve distribution (see Fig. 3D). In contrast, GStopo predominantly exhibited an inverted U-shaped curve across the almost entire brain, with no notable alterations in the age-related pattern following GVR (Fig. 3E–H). These results demonstrate that GVtopo and GStopo have opposing developmental trajectories and distinct spatial patterns.

### The GV can predict age better than GS, but it is even more accurate when combined with their topographies

Just as time variability shows robust predictive ability for age, GV exhibited a significantly higher predictive potential for age than GS ( $r^2$ : 0.243 VS. 0.007; see Fig. 4A). When incorporating their topographical maps, both GV and GS exhibited a similar level of predictive capability for age ( $r^2$ : 0.311 VS. 0.332). Furthermore, the combination of GV and GS only marginally enhanced predictive ability ( $r^2$ : 0.376), indicating that both topological structures may equally capture the developmental patterns of the brain. These results were duplicated with the independent SALD dataset (see Fig. 4B).

## Discussion

Delineating the developmental characteristics of brain function is a highly challenging problem. Our study demonstrated that GV and its topography are robust indicators, showing apparent sensitivity to age-related changes across the human lifespan. Notably, GV topography exhibited a U-shaped pattern of brain development, varying distinctly from medial to lateral regions, and this distribution was significantly different from that of GS topography. Moreover, the age-predictive power of GV was much stronger than that of GS. These findings highlight the potential of GV and its topography as markers for assessing brain maturation and aging, offering new insights into neural developmental processes.

### GV and GVtopo are reliable indices

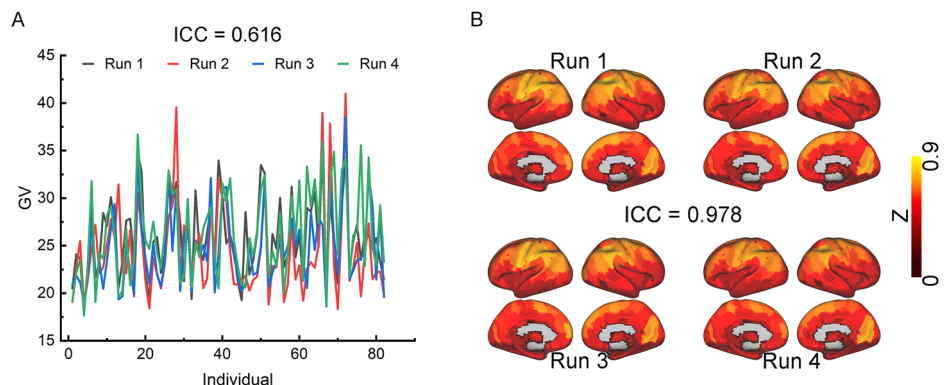
Various research fields, including neuroimaging, are confronting a severe crisis in reproducibility<sup>37</sup>. Here, the reliability of GV and GVtopo was established through ICC, which consistently exceeded 0.6 across the four runs of HCP data, outperforming the ICC for FC (ICC < 0.6) derived from the HCP test-retest dataset<sup>38,39</sup>. Such evidence points to the reproducibility of GV and GVtopo as measures of brain function.

### The non-linear relationship between age and GV

The positive quadratic relationship between GV and age, supported by robust measurements, aligns with existing evidence illustrating the dynamic age-related reorganization of the human brain<sup>40–43</sup>. White matter volume, for instance, follows a non-linear trajectory, peaking in the fifth decade of life. In contrast, the gray matter volume decreases gradually during the fourth and fifth decades of life, while the mean cortical thickness and total surface area diminish gradually until they stabilize after the age of 50 years<sup>44,45</sup>. These structural changes coincide with functional alterations in the brain, which adjust its architecture to maintain flexibility and efficiency in information processing<sup>46,47</sup>.

The synchronicity observed between the developmental trajectory of the GV and that of brain structure implies that the GV reflects the spatial complexity of the brain. This, in turn, mirrors the greater integration and lesser separation of brain networks in older adults, which reaches a relatively stable state around age 50<sup>46,48–50</sup>. Additionally, substantial evidence indicates that the temporal variability of brain signals is associated with cognitive

**Fig. 1 | The test-retest reliability of GV and GVtopo.** **A** The four colored dashes indicate the distribution of GV among the 82 subjects for the four Runs. The ICC of GV across the four runs is 0.616. **B** This panel presents the average GV topography across all subjects for each Run. Z-values were obtained using the Fisher z-transform of Pearson correlation coefficients. The ICC of GVtopo across the four runs is 0.978.



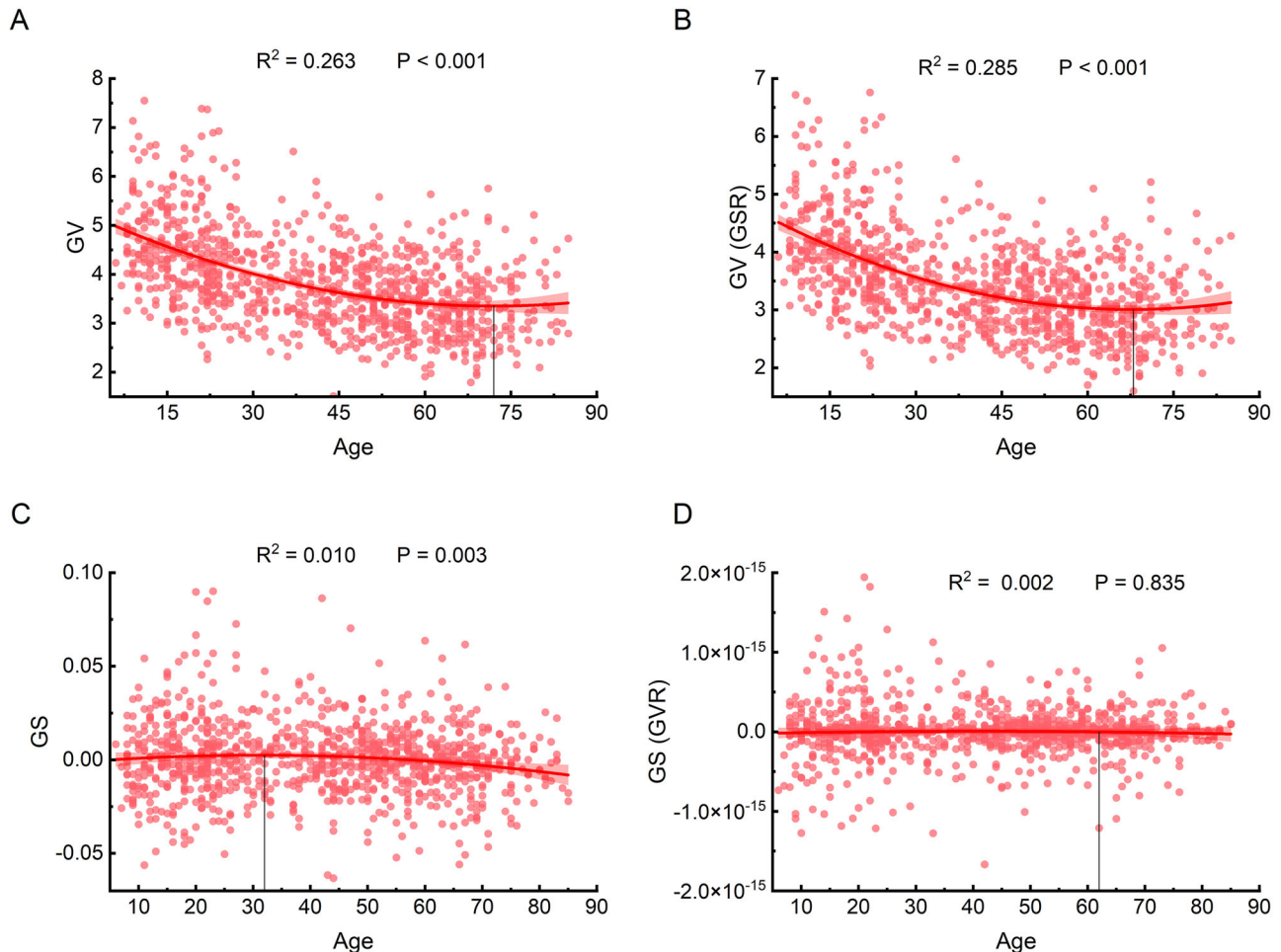


**Fig. 2 | Distinct relationships between GV/GS and age.** **A** The quadratic relationship between GV and age. **B** The quadratic relationship between GV and age after GSR. **C** The weak correlation between GS and age. **D** The correlation between

GS and age diminishes after GVR. The drop line of each subplot is labeled with the maximum/minimum value of the fitted curve.

flexibility, which is tuned by brain dynamics<sup>51</sup>. The similarity between the developmental trajectories of cognitive flexibility and GV suggests that spatial variability, like temporal variability, may play a role in cognitive adaptability<sup>50</sup>.

Moreover, numerous studies point to an age-related inflection point occurring between 35 and 55 years. This transition is primarily evident in higher-order cognitive functions such as arithmetic, comprehension, information, and vocabulary<sup>52</sup>, attentional functions like sustained attention<sup>53</sup> and conflict control<sup>54</sup>, and network properties such as global strength of within-network connectivity<sup>55</sup>, rich club architecture and network mean anatomical distance<sup>56</sup>, and the metabolic level of the basal forebrain cholinergic system<sup>42</sup>. The U-shaped changes observed in these brain and cognitive functions may reflect the brain's ongoing requirement for flexibility and stability across the lifespan, a hallmark of human intelligence and cognitive abilities<sup>57</sup>. In older adults, the observed increase in GV may signify a compensatory response, where heightened network variability is employed to counteract the decline in cognitive efficiency or to sustain functional capacity in the face of structural brain changes that come with aging<sup>23,25</sup>.

### Differentiated age patterns of GVtopo and GStopo

Our findings indicate that both GVtopo and GStopo are nonlinearly related to age, exhibiting either U-shaped or inverted U-shaped trajectories. This observation aligns with the nonlinear dynamics of the brain, suggesting that nonlinear functions are more effective in portraying the brain's developmental trajectory than linear models<sup>58</sup>. However, we also note that the age

trajectories of GVtopo and GStopo differ in the distribution of specific brain regions. From a developmental perspective, GS and GV topographies likely reflect complex, region-specific processes of development and aging within the brain<sup>23</sup>.

The inverted U-shaped pattern observed in GStopo has been associated with the maturation of brain networks during childhood and adolescence, where increased connectivity and integration across regions lead to a peak in global signal synchronization. In later adulthood, neurodegenerative processes, loss of synaptic density, and decreased efficiency of brain networks contribute to declines in cognitive function and neural synchrony<sup>45</sup>.

In contrast, GVtopo exhibits a different developmental trajectory, showing a U-shaped pattern in the medial frontoparietal (M-FPN) and lateral frontoparietal (L-FPN) networks, and an inverted U-shape in the midcingulo-insular (M-CIN) network. These networks are derived from the unified taxonomy proposed by Uddin et al., where M-FPN and L-FPN are labeled as control and default, respectively, while M-CIN is associated with salience<sup>59</sup>. Together, these networks facilitate cognitive flexibility and adaptability to changing life demands, which evolve significantly throughout an individual's life<sup>50</sup>.

Specifically, the GVtopo in M-FPN and L-FPN is lower in early and late life stages compared to middle age, indicating diminished modulation within these networks. This likely leads to increased reliance on crystallized knowledge and a decline in fluid cognitive skills<sup>60,61</sup>. Conversely, the positive polynomial trajectory of M-CIN may suggest that its global coordination mechanism for maintaining network function differs



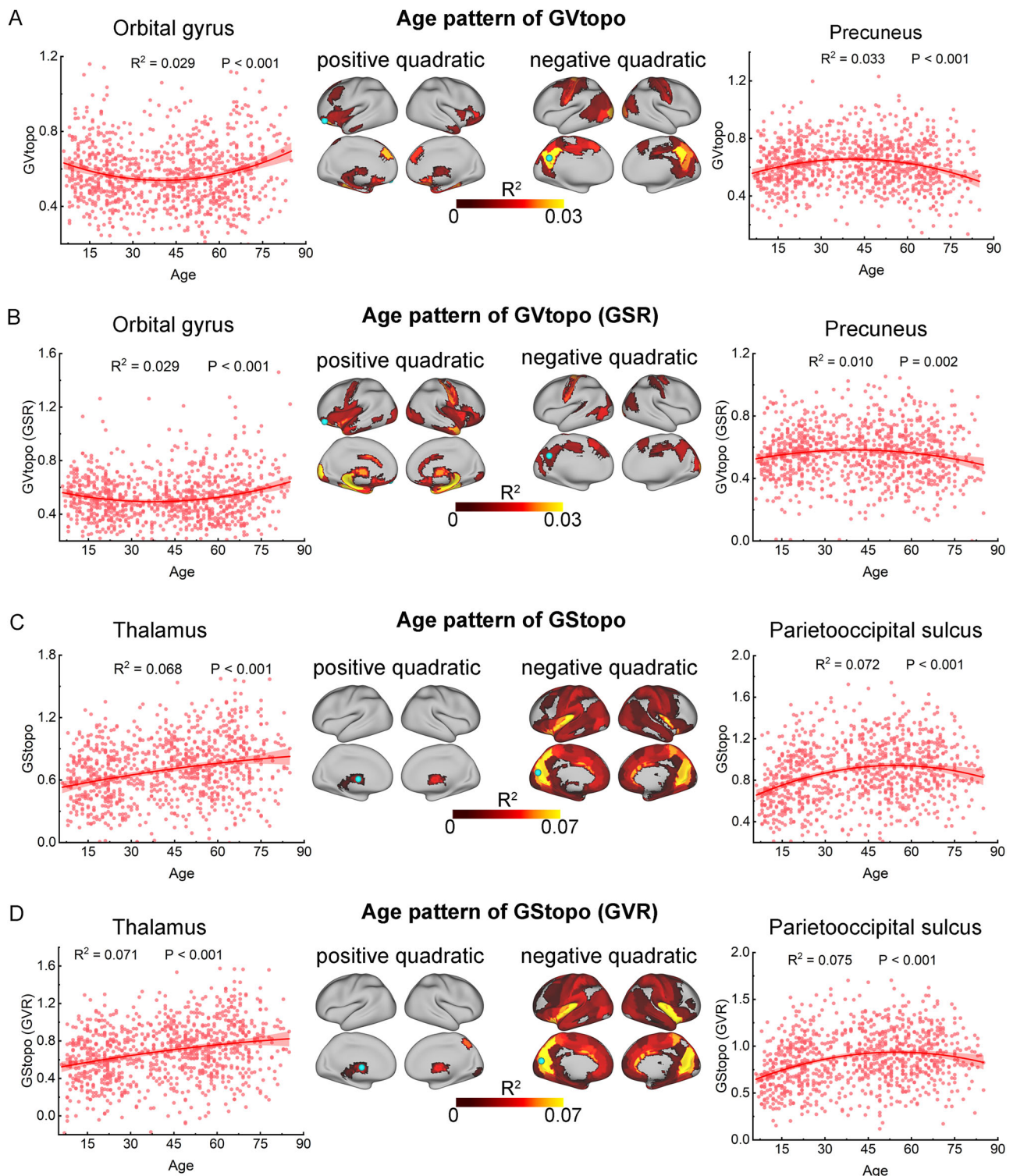


**Fig. 3 | The GVtopo primarily exhibits a positive quadratic relationship with age, whereas the GStopo mainly shows a negative quadratic relationship with age. A** The quadratic relationship between GVtopo and age. **B** The quadratic relationship

between GVtopo and age after GSR. **C** The quadratic relationship between GStopo and age. **D** The quadratic relationship between GStopo and age after GVR. The cyan dots in the brain map mark the brain regions with the highest  $R^2$  values.

from that of M-FPN and L-FPN. This hypothesis is supported by evidence from Zuo et al., who found that the M-CIN and FPN are not similarly engaged during memory encoding tasks, potentially explaining the observed age-related differences in background connectivity<sup>62</sup>. Furthermore, the pattern of decreasing and then increasing GVtopo in M-CIN may reflect a broader trend of differentiation and dedifferentiation within this network<sup>63</sup>.

### Effective age prediction using GV and GVtopo

The temporal variability of brain signals outperforms their temporal mean in predicting age<sup>64</sup>, as does the spatial variability compared to the spatial mean. This underscores the significance of brain signal variability, in both temporal and spatial dimensions, as a robust indicator of brain functional development and, potentially, of other brain functions and dysfunctions. The predictive performance increased when GS/GStopo and GV/GVtopo

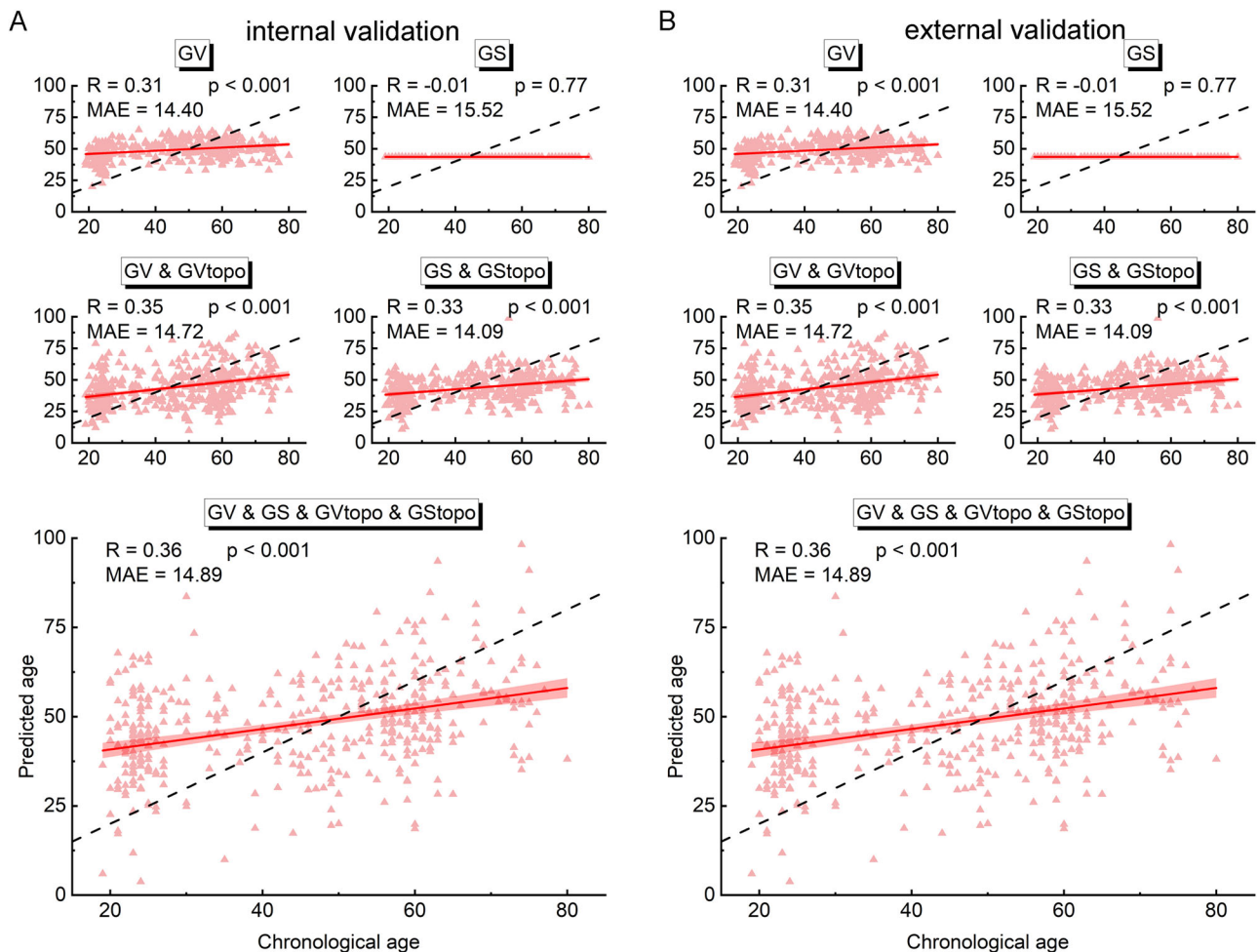


**Fig. 4 | Correlation of predicted age with actual age.** **A** The NKI-RS dataset was used as an internal validation with GV, GS, GVtopo, GSStopo, and the different combinations of them as predictive features, respectively. **B** Models trained on the NKI-RS dataset were used to predict the age of the subjects in the SALD dataset. The prediction performance is shown for the cases where GV, GS, GVtopo, GSStopo, and

the different combinations of them are used as predictive features respectively. The dash line in the scatterplot indicates  $y = x$ . NKI-RS The Nathan Kline Institute - Rockland Sample, SALD The Southwest University Adult Lifespan Dataset, MAE the mean absolute error.

were incorporated as additional features, suggesting that synchronization between global and local signals provides valuable complementary information for age prediction, which is not captured by individual global or local signals alone. Given the different timescales of local signals, global signals, and their synchronization<sup>17,65</sup>, a comprehensive understanding of brain function necessitates the consideration of the spatiotemporal dynamics of global topography.

We attained an R-value of 0.36 for the external validation in an independent dataset. It is worth noting that the validation sample lacks participants from the lower age range, whereas the metrics we examined demonstrate swift alterations within this age range. This discrepancy may underestimate the external validity. Nevertheless, the moderate effect size indicates that the metrics are not just artifacts of the specific sample but have broader applicability.

### Limitations

This study has several limitations. First, the explanation of GV's functionality, derived from its mathematical characteristics and age trajectory, is conjectural and necessitates verification in various contexts. Second, GV and its topography may be susceptible to physiological noises. Even though several denoising techniques have been utilized and their independence from GS and GSStopo has been proven, along with the revelation of their developmental trajectories, there is still a need for a systematic evaluation of the effects of various physiological noises on them.

### Conclusion

By utilizing large-scale lifespan datasets, we validated the robustness of global variability (GV) and its topography (GVtopo), demonstrating not only their reliability but also their ability to reveal distinct, non-linear trajectories of brain development that markedly diverge from traditional global signal (GS) measures. Additionally, these metrics show enhanced predictive accuracy for estimating age. This research signifies an advancement in our understanding of brain development, moving beyond conventional measures like GS by establishing GV as a refined and sensitive marker of neural changes over the course of the human lifespan. These works have advanced our understanding of the spatiotemporal structure of the brain<sup>66</sup>, offering new avenues for comprehending the dynamic changes in brain function from a spatiotemporal neuroscience perspective.

### Materials and methods

#### Dataset

We used the Human Connectome Project (HCP) 100 unrelated dataset<sup>67</sup> to validate GV reproducibility. The Nathan Kline Institute - Rockland Sample (NKI-RS) dataset<sup>68</sup> was used to explore the age effect of GV and the possibility of age prediction by GV. The reproducibility of the age prediction model was assessed using an independent Southwest University Adult Lifespan Dataset (SALD)<sup>69</sup>. All ethical regulations relevant to human research participants were followed.

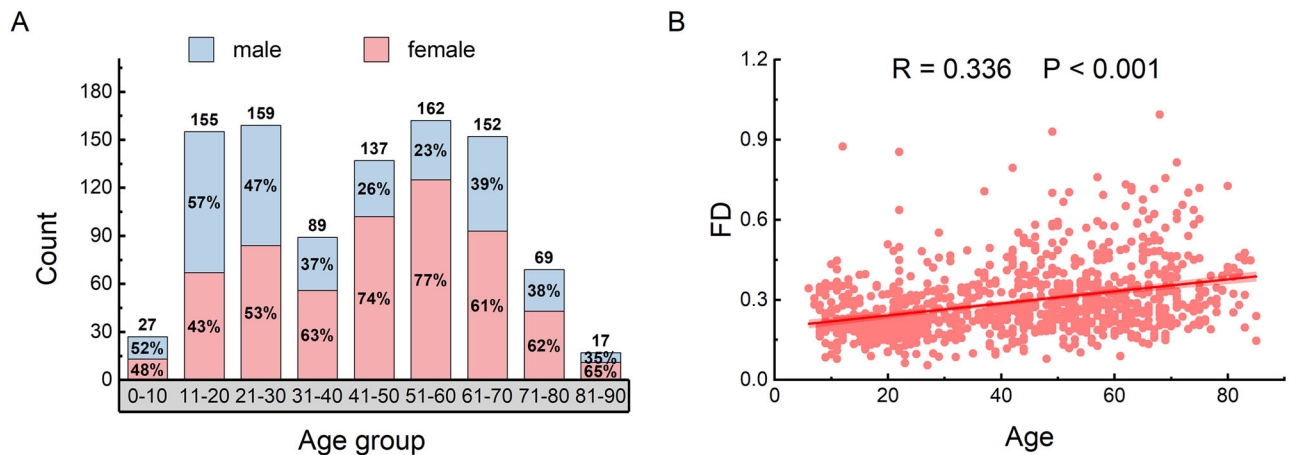


**Fig. 5 | Demographic information and the relationship between FD and age. A** Age and gender distribution. **B** Pearson's correlation between head motion and age.

The HCP dataset contains four runs of rs-fMRI data collected over two days, coded in left-to-right and right-to-left phases, respectively (i.e., REST1\_LR, REST1\_RL, REST2\_LR, and REST2\_RL). The local Institutional Review Board at Washington University in St. Louis approved the collection. Informed consent was obtained from all the participants. Details regarding recruitment and data collection are available at <https://www.humanconnectome.org>. We adopted data using a minimal preprocessing pipeline. These preprocessing steps include artifact removal, motion correction, and registration to the standard space. Linear trend, mean signal of Friston-24 parameters, white matter (WM), cerebrospinal fluid (CSF), and respiratory and cardiac noises were regressed out, smoothing with a full-width half-maximum (FWHM) of 6 mm, and temporal band-pass filtering (0.01–0.1 Hz). Resting-state fMRI image processing was performed using the DPARSF toolbox<sup>70</sup>.

NKI-RS is a large-scale lifespan sample (6–85 years old). The NKI Institutional Review Board approved the scanning protocol. Informed consent was obtained from all the participants. The details can be found at [http://fcon\\_1000.projects.nitrc.org/indi/enhanced](http://fcon_1000.projects.nitrc.org/indi/enhanced). The rs-fMRI data were preprocessed by removing the first ten time points, slice timing, realignment, normalization, nuisance regression (linear trend, Friston-24 parameters, WM, and CSF), smoothing (FWHM = 6 mm), and filtering (0.01–0.1 Hz).

The SALD contained a total of 492 volunteers (19–80 years old) recruited from SWU, China. This study was approved by the Research Ethics Committee of the Brain Imaging Center of SWU following the Declaration of Helsinki. Written informed consent was obtained from all the participants. The details can be found at [https://fcon\\_1000.projects.nitrc.org/indi/retro/sald.html](https://fcon_1000.projects.nitrc.org/indi/retro/sald.html). The preprocessing steps used were the same as those used for the NKI-RS dataset. Participants whose head motion of rotation was > 2.0 ° or translation > 2.0 mm were excluded.

### GS, GV, and their topography

For each participant, the GS/GV time series was obtained by calculating the mean and standard deviation of the signals overall gray matter voxels constrained by the binary BN\_Atlas\_246\_3 mm mask at each time point<sup>71</sup>. The GS topography is the Pearson correlation between the GS and local signals<sup>16,72</sup>. Similar to the calculation of GS topography, GV topography was calculated using the Pearson correlation between GV and the spatial variability of each brain region (the standard deviation of the signal values from all voxels within the region). The correlation coefficient  $r$  was transformed into Z-values (transformed) for subsequent analyses<sup>8,73</sup>.

### Reproducibility of GV

Using the HCP 100 dataset (<https://db.humanconnectome.org>), which contains four rs-MRI runs of the same participant, test-retest reliabilities of GV (represented by the mean value of GV time series), and GV topography

were quantified by the intraclass correlation coefficient (ICC) among different runs<sup>74</sup> that have been adopted in a wide range of fMRI studies<sup>75–77</sup>. The ICC can be calculated using the following formula:

$$ICC = \frac{MS_b - MS_w}{MS_b + (k - 1)MS_w}$$

where  $MS_b$  represents the mean square between subjects,  $MS_w$  represents the mean square within subjects, and  $k = 4$  indicates the number of measurements. In this study, we categorized ICC values into four intervals: poor reliability (< 0.4), fair reliability (0.4–0.6), good reliability (0.6–0.8), and excellent reliability (0.8–1.0)<sup>78</sup>. In practice, we believe that GV and GVtopo exhibit reliability greater than fair, with ICC values exceeding 0.4<sup>79</sup>.

### Age effect analysis

Using the NKI-RS dataset, we initially examined the correlation between frame-wise displacement (FD)<sup>80</sup> and age. We observed a positive association in which subject head movement increased as age increased, as shown in Fig. 5. To mitigate the influence of head movement on the age effect of the global indicator, we performed a regression analysis that included head movement as a covariate alongside gender. Subsequently, we conduct an analysis by examining the residuals. To examine the age-related trajectories of GV, GS, and their topography, we fitted both linear and quadratic polynomial models. The quadratic model is defined as  $y = \beta_0 + \beta_1 x + \beta_2 x^2$ , where  $y$  represents GV, GS, or their topographic values,  $x$  represents age, and  $\beta_2$  is the quadratic coefficient. Trajectories were classified based on the sign of  $\beta_2$ : a positive  $\beta_2$  indicated a U-shaped trajectory, and a negative  $\beta_2$  an inverted U-shape. We selected the model with the highest explained variance ( $R^2$ ) to characterize the developmental pattern of each measure.

### Age prediction

The age was predicted using a quadratic kernel-based support vector regression (SVR) model with a default error penalty factor ( $c = 1$ ). The features utilized for prediction included various integrations of GV, GS, GVtopo, and GSstopo. The model was initially validated internally using the NKI-RS dataset. To assess the model's predictive performance, a 10-fold cross-validation approach was employed with 100 repetitions. In each repetition, the dataset was randomly divided into 10 subsets, with one subset held out for validation while the remaining nine subsets were used for training. This process was repeated 100 times, and performance metrics were averaged over these iterations. The evaluation metrics included the mean Pearson's correlation coefficient between the actual and predicted ages ( $R$ ) and the mean absolute error (MAE).

Following this internal validation, we created a consensus model for external validation to evaluate the model's ability to generalize to new data.



This involved training the model on the entire NKI-RS dataset and then using it to predict subjects' ages in the SALD dataset. The R and the MAE for all subjects in the SALD dataset were used to assess the model's performance. This cross-dataset prediction helped test the model's robustness and the selected features' effectiveness in predicting age across different datasets.

### Statistics and reproducibility

The statistical analyses employed several robust methodologies to ensure the reliability and validity of the findings. Intraclass correlation coefficients were used to assess the reliability of GV and GVtopo across four independent scans, giving a comprehensive evaluation of their consistency. Both linear and nonlinear models were applied to model the developmental trajectories of GV/GS, allowing for a nuanced comparison of age-related patterns reflected in these metrics. Additionally, an independent sample was utilized for external validation to rigorously evaluate the predictive power of GV in estimating individuals' ages. This approach effectively demonstrated the generalizability and robustness of the predictive model beyond the original dataset. Furthermore, we provide the analysis procedure along with the corresponding code to ensure the reproducibility of the results, enhancing the transparency and credibility of our findings.

### Reporting summary

Further information on research design is available in the Nature Portfolio Reporting Summary linked to this article.

### Data availability

The original datasets used in this study are publicly accessible (see <https://db.humanconnectome.org>, [https://fcon\\_1000.projects.nitrc.org/indi/pro/nki.html](https://fcon_1000.projects.nitrc.org/indi/pro/nki.html), [http://fcon\\_1000.projects.nitrc.org/indi/retro/sald.html](http://fcon_1000.projects.nitrc.org/indi/retro/sald.html)).

### Code availability

The code involved can be obtained from <https://doi.org/10.5281/zenodo.15003714><sup>81</sup>.

Received: 21 October 2024; Accepted: 13 March 2025;

Published online: 26 March 2025

### References

- Deco, G., Cruzat, J. & Kringelbach, M. L. Brain songs framework used for discovering the relevant timescale of the human brain. *Nat. Commun.* **10**, 583 (2019).
- Coquelet, N. et al. Changes in electrophysiological static and dynamic human brain functional architecture from childhood to late adulthood. *Sci. Rep.* **10**, 18986 (2020).
- Ferreira, L. K. & Busatto, G. F. Resting-state functional connectivity in normal brain aging. *Neurosci. Biobehav. Rev.* **37**, 384–400 (2013).
- Xia, Y. et al. Tracking the dynamic functional connectivity structure of the human brain across the adult lifespan. *Hum. Brain Mapp.* **40**, 717–728 (2019).
- Dong, J. et al. Hurst Exponent Analysis of Resting-State fMRI Signal Complexity across the Adult Lifespan. *Front. Neurosci.* **12**, 34 (2018).
- Vij, S. G., Nomi, J. S., Dajani, D. R. & Uddin, L. Q. Evolution of spatial and temporal features of functional brain networks across the lifespan. *Neuroimage* **173**, 498–508 (2018).
- Murphy, K. & Fox, M. D. Towards a consensus regarding global signal regression for resting state functional connectivity MRI. *Neuroimage* **154**, 169–173 (2017).
- Power, J. D., Plitt, M., Laumann, T. O. & Martin, A. Sources and implications of whole-brain fMRI signals in humans. *Neuroimage* **146**, 609–625 (2017).
- Bello, M. E. et al. Dynamic resting state fMRI analysis in mice reveals a set of Quasi-Periodic Patterns and illustrates their relationship with the global signal. *Neuroimage* **180**, 463–484 (2018).
- Ma, Y., Ma, Z., Liang, Z., Neuberger, T. & Zhang, N. Global brain signal in awake rats. *Brain Struct. Funct.* **225**, 227–240 (2020).
- Scholvinck, M. L., Maier, A., Ye, F. Q., Duyn, J. H. & Leopold, D. A. Neural basis of global resting-state fMRI activity. *Proc. Natl Acad. Sci.* **107**, 10238–10243 (2010).
- Liu, X. et al. Arousal transitions in sleep, wakefulness, and anesthesia are characterized by an orderly sequence of cortical events. *Neuroimage* **116**, 222–231 (2015).
- Leopold, D. A., Murayama, Y. & Logothetis, N. K. Very slow activity fluctuations in monkey visual cortex: implications for functional brain imaging. *Cereb. Cortex* **13**, 422–433 (2003).
- Li, J. et al. Topography and behavioral relevance of the global signal in the human brain. *Sci. Rep.* **9**, 14286 (2019).
- Ao, Y., Ouyang, Y., Yang, C. & Wang, Y. Global Signal Topography of the Human Brain: A Novel Framework of Functional Connectivity for Psychological and Pathological Investigations. *Front. Hum. Neurosci.* **15**, 644892 (2021).
- Zhang, J., Huang, Z., Tumati, S. & Northoff, G. Rest-task modulation of fMRI-derived global signal topography is mediated by transient coactivation patterns. *PLoS Biol.* **18**, e3000733 (2020).
- Wang, Y. et al. Frequency-dependent effective connections between local signals and the global brain signal during resting-state. *Cogn. Neurodyn.* **17**, 555–560 (2023).
- Wong, C. W., Olafsson, V., Tal, O. & Liu, T. T. The amplitude of the resting-state fMRI global signal is related to EEG vigilance measures. *Neuroimage* **83**, 983–990 (2013).
- Gutierrez-Barragan, D., Basson, M. A., Panzeri, S. & Gozzi, A. Infraslow State Fluctuations Govern Spontaneous fMRI Network Dynamics. *Curr. Biol.* **29**, 2295–2306.e2295 (2019).
- Tanabe, S. et al. Altered Global Brain Signal during Physiologic, Pharmacologic, and Pathologic States of Unconsciousness in Humans and Rats. *Anesthesiology* **132**, 1392–1406 (2020).
- Huang, Z. et al. Decoupled temporal variability and signal synchronization of spontaneous brain activity in loss of consciousness: An fMRI study in anesthesia. *Neuroimage* **124**, 693–703 (2016).
- Scalabrini, A. et al. All roads lead to the default-mode network-global source of DMN abnormalities in major depressive disorder. *Neuropsychopharmacology* **45**, 2058–2069 (2020).
- Ao, Y. et al. Spatiotemporal dedifferentiation of the global brain signal topography along the adult lifespan. *Hum. Brain Mapp.* **44**, 5906–5918 (2023).
- Nomi, J. S. et al. Global fMRI signal topography differs systematically across the lifespan. *bioRxiv*, 2022.2007.2027.501804, <https://doi.org/10.1101/2022.07.27.501804> (2022).
- Ao, Y. et al. The temporal dedifferentiation of global brain signal fluctuations during human brain ageing. *Sci. Rep.* **12**, 3616 (2022).
- Halliday, D. W. R. et al. Mean and variability in functional brain activations differentially predict executive function in older adults: an investigation employing functional near-infrared spectroscopy. *Neurophotonics* **5**, 011013 (2018).
- Zhang, P. W. et al. Distinction Between Variability-Based Modulation and Mean-Based Activation Revealed by BOLD-fMRI and Eyes-Open/Eyes-Closed Contrast. *Front. Neurosci.* **12**, 516 (2018).
- Grady, C. L. & Garrett, D. D. Brain signal variability is modulated as a function of internal and external demand in younger and older adults. *Neuroimage* **169**, 510–523 (2018).
- Wang, Y. et al. Spatial complexity of brain signal is altered in patients with generalized anxiety disorder. *J. Affect. Disord.* **246**, 387–393 (2019).
- Wang, Y. et al. Spatial variability of low frequency brain signal differentiates brain states. *PLoS One* **15**, e0242330 (2020).
- O'Hearn, K., Larsen, B., Fedor, J., Luna, B. & Lynn, A. Representational similarity analysis reveals atypical age-related changes in brain regions supporting face and car recognition in autism. *NeuroImage* **209**, 116322 (2020).

32. Zarahn, E., Aguirre, G. K. & D'Esposito, M. Empirical analyses of BOLD fMRI statistics. I. Spatially unsmoothed data collected under null-hypothesis conditions. *Neuroimage* **5**, 179–197 (1997).
33. Yang, G. J. et al. Altered global brain signal in schizophrenia. *Proc. Natl Acad. Sci.* **111**, 7438–7443 (2014).
34. Noble, S., Scheinost, D. & Constable, R. T. A decade of test-retest reliability of functional connectivity: A systematic review and meta-analysis. *Neuroimage* **203**, 116157 (2019).
35. Elliott, M. L. et al. What is the test-retest reliability of common task-functional MRI measures? New empirical evidence and a meta-analysis. *Psychol. Sci.* **31**, 792–806 (2020).
36. Zhang, J. & Northoff, G. Beyond noise to function: reframing the global brain activity and its dynamic topography. *Commun. Biol.* **5**, 1350 (2022).
37. Begley, C. G. & Ioannidis, J. P. A. Reproducibility in Science. *Circulation Res.* **116**, 116–126 (2015).
38. Zhang, C., Baum, S. A., Adduru, V. R., Biswal, B. B. & Michael, A. M. Test-retest reliability of dynamic functional connectivity in resting state fMRI. *Neuroimage* **183**, 907–918 (2018).
39. Galazzo, I. B. et al. in *2021 IEEE 18th International Symposium on Biomedical Imaging (ISBI)*. 1860–1863 (IEEE).
40. Arshad, M., Stanley, J. A. & Raz, N. Adult age differences in subcortical myelin content are consistent with protracted myelination and unrelated to diffusion tensor imaging indices. *Neuroimage* **143**, 26–39 (2016).
41. Burianova, H., Lee, Y., Grady, C. L. & Moscovitch, M. Age-related dedifferentiation and compensatory changes in the functional network underlying face processing. *Neurobiol. Aging* **34**, 2759–2767 (2013).
42. Cichocka, M. & Beres, A. From fetus to older age: A review of brain metabolic changes across the lifespan. *Ageing Res Rev.* **46**, 60–73 (2018).
43. Koen, J. D., Sroková, S. & Rugg, M. D. Age-related neural dedifferentiation and cognition. *Curr. Opin. Behav. Sci.* **32**, 7–14 (2020).
44. Lebel, C. et al. Diffusion tensor imaging of white matter tract evolution over the lifespan. *Neuroimage* **60**, 340–352 (2012).
45. Bethlehem, R. A. et al. Brain charts for the human lifespan. *Nature* **604**, 525–533 (2022).
46. Deery, H. A., Di Paolo, R., Moran, C., Egan, G. F. & Jamadar, S. D. The older adult brain is less modular, more integrated, and less efficient at rest: A systematic review of large-scale resting-state functional brain networks in aging. *Psychophysiology* **60**, e14159 (2023).
47. Reuter-Lorenz, P. A. & Park, D. C. How does it STAC up? Revisiting the scaffolding theory of aging and cognition. *Neuropsychol. Rev.* **24**, 355–370 (2014).
48. Bagarinao, E. et al. An unbiased data-driven age-related structural brain parcellation for the identification of intrinsic brain volume changes over the adult lifespan. *Neuroimage* **169**, 134–144 (2018).
49. Niu, Y. et al. Trajectories of brain entropy across lifetime estimated by resting state functional magnetic resonance imaging. *Hum. Brain Mapp.* **43**, 4359–4369 (2022).
50. Kupis, L. et al. Brain Dynamics Underlying Cognitive Flexibility Across the Lifespan. *Cereb. Cortex* **31**, 5263–5274 (2021).
51. Armbruster-Genc, D. J. N., Ueltzhöffer, K. & Fiebach, C. J. Brain Signal Variability Differentially Affects Cognitive Flexibility and Cognitive Stability. *J. Neurosci.* **36**, 3978 (2016).
52. Hartshorne, J. K. & Germine, L. T. When does cognitive functioning peak? The asynchronous rise and fall of different cognitive abilities across the life span. *Psychol. Sci.* **26**, 433–443 (2015).
53. Fortenbaugh, F. C. et al. Sustained Attention Across the Life Span in a Sample of 10,000: Dissociating Ability and Strategy. *Psychol. Sci.* **26**, 1497–1510 (2015).
54. Waszak, F., Li, S. C. & Hommel, B. The development of attentional networks: cross-sectional findings from a life span sample. *Dev. Psychol.* **46**, 337–349 (2010).
55. Edde, M., Leroux, G., Altena, E. & Chanraud, S. Functional brain connectivity changes across the human life span: From fetal development to old age. *J. Neurosci. Res.* **99**, 236–262 (2021).
56. Cao, M. et al. Topological organization of the human brain functional connectome across the lifespan. *Dev. Cogn. Neurosci.* **7**, 76–93 (2014).
57. Ionescu, T. Exploring the nature of cognitive flexibility. *N. Ideas Psychol.* **30**, 190–200 (2012).
58. Rabinovich, M. I. & Muezzinoglu, M. K. Nonlinear dynamics of the brain: emotion and cognition. *Phys.-Uspekhi* **53**, 357 (2010).
59. Uddin, L. Q., Yeo, B. T. T. & Spreng, R. N. Towards a Universal Taxonomy of Macro-scale Functional Human Brain Networks. *Brain Topogr.* **32**, 926–942 (2019).
60. Spreng, R. N. et al. Semanticized autobiographical memory and the default - executive coupling hypothesis of aging. *Neuropsychologia* **110**, 37–43 (2018).
61. Turner, G. R. & Spreng, R. N. Prefrontal Engagement and Reduced Default Network Suppression Co-occur and Are Dynamically Coupled in Older Adults: The Default-Executive Coupling Hypothesis of Aging. *J. Cogn. Neurosci.* **27**, 2462–2476 (2015).
62. Zuo, N. et al. Activation-based association profiles differentiate network roles across cognitive loads. *Hum. Brain Mapp.* **40**, 2800–2812 (2019).
63. Fjell, A. M. et al. Critical ages in the life course of the adult brain: nonlinear subcortical aging. *Neurobiol. Aging* **34**, 2239–2247 (2013).
64. Garrett, D. D., Kovacevic, N., McIntosh, A. R. & Grady, C. L. Blood Oxygen Level-Dependent Signal Variability Is More than Just Noise. *J. Neurosci.* **30**, 4914 (2010).
65. Mitra, A. et al. Spontaneous Infra-slow Brain Activity Has Unique Spatiotemporal Dynamics and Laminar Structure. *Neuron* **98**, 297–305.e296 (2018).
66. Wang, Y., Zhang, C., Liu, Q. & Jing, X. The intrinsic spatiotemporal structure of cognitive functions inspires the intervention of brain functions. *Front. Neurol.* **16**, 1494673 (2025).
67. Van Essen, D. C. et al. The WU-Minn Human Connectome Project: an overview. *Neuroimage* **80**, 62–79 (2013).
68. Nooner, K. B. et al. The NKI-Rockland Sample: A Model for Accelerating the Pace of Discovery Science in Psychiatry. *Front. Neurosci.* **6**, 152 (2012).
69. Wei, D. et al. Structural and functional brain scans from the cross-sectional Southwest University adult lifespan dataset. *Sci. Data* **5**, 180134 (2018).
70. Yan, C. & Zang, Y. DPARSF: a MATLAB toolbox for “pipeline” data analysis of resting-state fMRI. *Front. Syst. Neurosci.* **13**, <https://doi.org/10.3389/fnsys.2010.00013> (2010).
71. Fan, L. et al. The Human Brainnetome Atlas: A New Brain Atlas Based on Connectional Architecture. *Cereb. Cortex* **26**, 3508–3526 (2016).
72. Fox, M. D., Zhang, D., Snyder, A. Z. & Raichle, M. E. The global signal and observed anticorrelated resting state brain networks. *J. Neurophysiol.* **101**, 3270–3283 (2009).
73. Fisher, R. A. Frequency Distribution of the Values of the Correlation Coefficient in Samples from an Indefinitely Large Population. *Biometrika* **10**, 507–521 (1915).
74. Shrout, P. E. & Fleiss, J. L. Intraclass correlations: uses in assessing rater reliability. *Psychol. Bull.* **86**, 420–428 (1979).
75. Caceres, A., Hall, D. L., Zelaya, F. O., Williams, S. C. & Mehta, M. A. Measuring fMRI reliability with the intra-class correlation coefficient. *Neuroimage* **45**, 758–768 (2009).
76. Telesford, Q. K. et al. Reproducibility of graph metrics in FMRI networks. *Front. Neuroinform.* **4**, 117 (2010).
77. Thomason, M. E. et al. Resting-state fMRI can reliably map neural networks in children. *Neuroimage* **55**, 165–175 (2011).
78. Cicchetti, D. V. The precision of reliability and validity estimates revisited: distinguishing between clinical and statistical significance of sample size requirements. *J. Clin. Exp. Neuropsychol.* **23**, 695–700 (2001).



79. Yang, L. et al. Test–Retest Reliability of Synchrony and Metastability in Resting State fMRI. *Brain Sci.* **12**, 66 (2022).
80. Power, J. D., Barnes, K. A., Snyder, A. Z., Schlaggar, B. L. & Petersen, S. E. Spurious but systematic correlations in functional connectivity MRI networks arise from subject motion. *Neuroimage* **59**, 2142–2154 (2012).
81. Yang, C. The lifelong nonlinear development of spatial variability of brain signals. *Zenodo* <https://doi.org/10.5281/zenodo.15003715> (2025).

## Acknowledgements

This study was supported by the National Nature Science Foundation of China (Grant No.62177035, 32471101) and Sichuan Science and Technology Program (2024NSFSC2086).

## Author contributions

Y.W. designed the study. C.Y. and G.L. analyzed the data. Y.W., C.Y., G.L., X.J., J.Y., and G.N. wrote the manuscript. All authors reviewed and edited the manuscript. All authors read and approved the manuscript.

## Competing interests

The authors declare no competing interests.

## Additional information

**Supplementary information** The online version contains supplementary material available at <https://doi.org/10.1038/s42003-025-07939-7>.

**Correspondence** and requests for materials should be addressed to Yifeng Wang.

**Peer review information** *Communications Biology* thanks Afra Wohlschlaeger and Pablo Barttfeld for their contribution to the peer review of this work. Primary Handling Editor: Jasmine Pan. A peer review file is available.

**Reprints and permissions information** is available at <http://www.nature.com/reprints>

**Publisher's note** Springer Nature remains neutral with regard to jurisdictional claims in published maps and institutional affiliations.

**Open Access** This article is licensed under a Creative Commons Attribution-NonCommercial-NoDerivatives 4.0 International License, which permits any non-commercial use, sharing, distribution and reproduction in any medium or format, as long as you give appropriate credit to the original author(s) and the source, provide a link to the Creative Commons licence, and indicate if you modified the licensed material. You do not have permission under this licence to share adapted material derived from this article or parts of it. The images or other third party material in this article are included in the article's Creative Commons licence, unless indicated otherwise in a credit line to the material. If material is not included in the article's Creative Commons licence and your intended use is not permitted by statutory regulation or exceeds the permitted use, you will need to obtain permission directly from the copyright holder. To view a copy of this licence, visit <http://creativecommons.org/licenses/by-nc-nd/4.0/>.

© The Author(s) 2025